J Petrol Explor Prod Technol (2018) 8:117–130
https://doi.org/10.1007/s13202-017-0394-3

ORIGINAL PAPER - EXPLORATION GEOPHYSICS

Characterizing fluid contacts by joint inversion of seismic P-wave impedance and velocity

Amjad Ali[1] · **Abdullatif A. Al-Shuhail**[1]

Received: 21 December 2016 / Accepted: 24 September 2017 / Published online: 9 October 2017

Abstract In the past, seismic exploration technique was mainly used for gathering information about subsurface rock structures and fluids by analyzing the travel time, reflection amplitude, and phase variations. However, nowadays, many additional seismic attributes have been introduced by the seismic interpreters, which aid in the visualization of subsurface geological structures, facies, and lithologies. This research aims to identify the pore fluids in the reservoir using post-stacked seismic data without requiring well log data. Gassmann's equation, a well-known equation for fluid substitution, has been used for fluid substitution in this research. To test the proposed technique, a three-layer geological anticline model has been used. The third layer of the model represents a reservoir which is saturated with water, except its top part which is fully saturated with petroleum. Fluid identification is achieved by using fluid density, velocity changes, and acoustic impedance (AI). P-wave velocity and AI are measured from post-stacked seismic data and its inversion, from which the saturated rock density and compressional modulus (M) are calculated. Using this information, saturated rock density and compressional modulus are inverted for fluid velocity and density, respectively, to identify the pore fluid.

Keywords Gassmann's equation · Fluid Density and velocity changes · Oil-water contact · Fluid substitution · Fluid identification

✉ Amjad Ali
amjadjan_87@yahoo.com

Abdullatif A. Al-Shuhail
ashuhail@kfupm.edu.sa

[1] Geosciences Department, College of Petroleum Engineering and Geosciences, King Fahd University of Petroleum and Minerals, Dhahran, Saudi Arabia

Introduction

Petrophysicists normally use well logs data in oil and gas industry to identify pore fluids and mark fluid contacts at reservoir level, which is an essential part of reserves estimation and economics. During hydrocarbon exploration, explorers look for a subsurface structure with high porosity because the hydrocarbon tends to accumulate in these structures. Normally spots, where hydrocarbon accumulates, have relatively low acoustic velocity, density, and AI. These are good indicators of the presence of hydrocarbon. This study investigates the effects of pore fluids on seismic data in order to characterize the pore fluid. Characterization of fluids at reservoir level by using seismic data in the absence of well logs data could be a very helpful tool in the development of new oil and gas fields. It could also help in reserves estimation before drilling new wells and will increase the chances of success.

In a typical hydrocarbon reservoir, the gas is commonly found in the top most part followed by oil that sits on top of the water. This sequence is mainly caused by the difference in densities of reservoir fluids. There is often a sharp contact among gas-, oil-, and water-saturated zones of the reservoir, which are referred to as the oil–water contact (OWC), gas-oil contact (GOC), or gas–water contact (GWC). The identification of fluids at the reservoir and the marking of this OWC/GOC/GWC are essential for the volumetric calculation of oil reserves of an oil reservoir (Chombart 1960). For example, for the computation of water saturation (Sw), one needs to define OWC in a wellbore.

To identify and mark the OWC/GOC/GWC, different techniques such as mud logs, core analysis, resistivity log, and neutron log have been developed in the past. Many developments have taken place in the field of well logging

in the last 25 years. Archie (1942) was the first person who defined the term "petrophysics," and now it has become the science of borehole geophysics (Snyder and Fleming 1985). Gevers and Watson (1978) proposed three-stage process for quantitative interpretation of the formation using the well log data. In the first stage, this approach generates acoustic log data for every 0.5 ft and then calibrates the acoustic log data with AI and at the third and final stages calculates and collects the rock physics parameters and also generates a graph for the variation of density and velocity with depth to delineate the hydrocarbon zones.

In Campos Basin, Brazil, anomalous amplitudes were found just below the target horizon. Initially, it was assumed that this is due to lithological changes in the vertical direction, but later it was found that the position of these anomalous amplitudes was present at the depth of OWC, which was confirmed by well log data. Later, it was concluded that it was caused by a change in AI due to fluid change. To confirm this hypothesis, they used the Biot–Geertsma equation for frequency. Finally, the measured values were incorporated to match the velocities for both water- and oil-saturated zones. Then, the seismic data were reinforced with the modeling data; as a result, the target reflector disappeared and a prominent reflector appeared which coincided with the OWC of the nearest well (Rosa et al. 1985).

Williams (1990) developed an algorithm for hydrocarbon identification, which he named acoustic log hydrocarbon indicator (ALHI). Basically, this algorithm is applied to clastic rocks, where the aim is to differentiate the water-bearing zone from the hydrocarbon-bearing zone. Klimentos (1995) used three well data to gauge the P- and S-wave attenuation from sonic data using the spectral peak method. Due to P- and S-wave attenuation, a gas condensate in clean sandstone was marked with the Sw ranging from 25 to 30%.

Chiburis (1984, 1987) worked on the idea of AVO application in Saudi Arabia for pore fluid characterization in the reservoir and detecting OWC. For this study, six different areas have been investigated. Three of these areas are offshore, and the remaining three are onshore in the eastern province of Saudi Arabia. One of these areas is marine area 2, which has an oil carbonate reservoir at a depth of 2400 m. There are two structures present in this area, and both are oil reservoir followed by brine. AVO inversion for three lines on both structures gave positive AVO and was able to delineate the OWC for both structures.

Kim et al. (2004) worked on the idea of simultaneous AVO inversion to estimate the subsurface rock properties such as AI, Poisson's ratio, shear impedance, and density. In AVO, the angle of incident is an important parameter and it is obtained from seismic processing velocities.

Andrew et al. (2004) did the AVO analysis for Bin Nevis Reservoir, Canada, to find the API variation in the reservoir and differentiate the pore fluid in the reservoir. Using the fluid factor analysis gave the picture of the reservoir and showed the boundary between the oil and water. The cross-plot of P- and S-wave reflectivity series separated the two different pore fluids in the reservoir.

Chi and Han (2007) studied the reservoir properties using the AVO attributes. They linked the rock physics with AVO attributes to understand the reservoir properties. They used the Gassmann's equation for fluid identification and rock physics relationship for fluid modulus. Through the AVO attributes, the clay content, Sw, and porosity were estimated. They used the shaley-sand model, in which they computed the elastic properties of the model. They applied the AVO inversion through which they got the P- and S-wave velocities, which is later linked with the rock physics model for the detailed picture of the reservoir.

Kato and Stewart (2012) did the AVO inversion for time-lapse elastic reservoir properties. In time-lapse data, they did the AVO inversion for both baselines and monitor survey data to obtain simultaneously elastic properties such as P-wave, S-wave, velocities, and density along with the uncertainties. During the inversion, they used the individual wavelet for both data sets. The final results reasonably agreed with well log data.

Li and Zhang (2015) did the direct estimation of petrophysical properties from AVO inversion. They interlinked the rock physics model and AVO inversion attributes to get information about reservoir properties. Initially, they did the linear regression analysis of the well data to obtain the rock physics model, and then, they obtained the reflection coefficient (RC) equation for the incorporation of the rock physics model with Aki's RC. Finally, the AVO inversion was done for reservoir parameters.

Methodology

Figure 1 describes the adopted methodology for developing the model, inversion steps and finally the identification of the pore fluid. The geological model that is comprised of three layers, its synthetic seismic model, and the trace at the middle of the reservoir are given in Figs. 2, 3, and 4, respectively. In the geological model, the surface to the top of the second layer is assumed as one layer, the second layer is shale that acts as a cap rock, and the third layer is pure sandstone that is the reservoir in this model. The lateral extension of the model is 4000 m, and the vertical depth is 3000 m. The maximum curvature of the geological

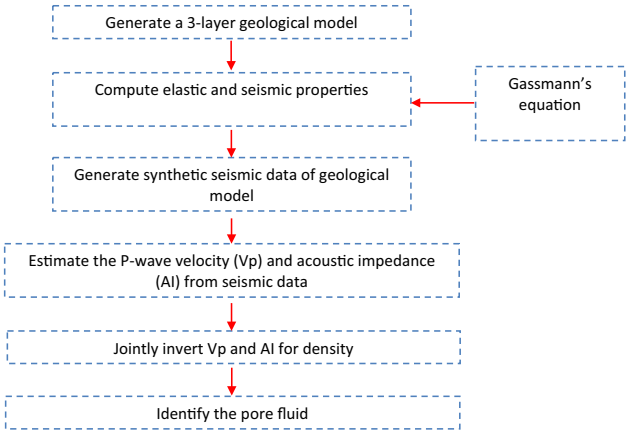

Fig. 1 Flowchart of the proposed inversion

model is 400 m at the reservoir level, where the maximum thickness of oil column in the reservoir is 200 m and the remaining part is fully water saturated.

For fluid substitution, the Gassmann's equation has been used. To compute the elastic and seismic properties, Batzle and Wang equations, 1992 were used. The computed elastic properties, i.e., fluid modulus, dry rock and saturated rock modulus, and seismic properties, i.e., fluid velocity, fluid density and P-wave velocity, are given in Tables 1, 2, 3, 4, 5, and 6, respectively. Using density and P-wave velocity, a synthetic seismogram was generated. This synthetic model was then used for inversion purpose.

Fluid properties

In this paper, Gassmann's equation is used for fluid substitution to observe the effects on seismic properties due to pore fluid. Three different fluids (gas, live oil, and water) are used to compute the seismic and elastic properties of the reservoir fluid. The properties of these three fluids are computed and described below.

Gas properties

Gas is generally characterized by the ratio of gas density to air density. In this study, methane gas has been used for fluid substitution and its specific gravity is 0.56. The density of the gas is calculated using following empirical equations. In first step, absolute temperature is determined using the following Kelvin equation:

$$T_a = T + 273 \tag{1}$$

where T_a is the absolute temperature (Kelvin) and T is 150 °C (assumed) temperature at the reservoir level. The pressure in MPa at the reservoir level is computed using pressure water gradient equation:

$$P = ((D \times 0.433) + 14.7) \times 0.006894757293178 \times 3.28 \tag{2}$$

where P is the pressure (psi) and D is the depth (m). Next, pseudo-pressure and pseudo-temperature were determined using following equation, (Batzle and Wang 1992):

$$P_r = \frac{P}{4.892 - 0.4048 \times G} \tag{3}$$

Fig. 2 Geological model

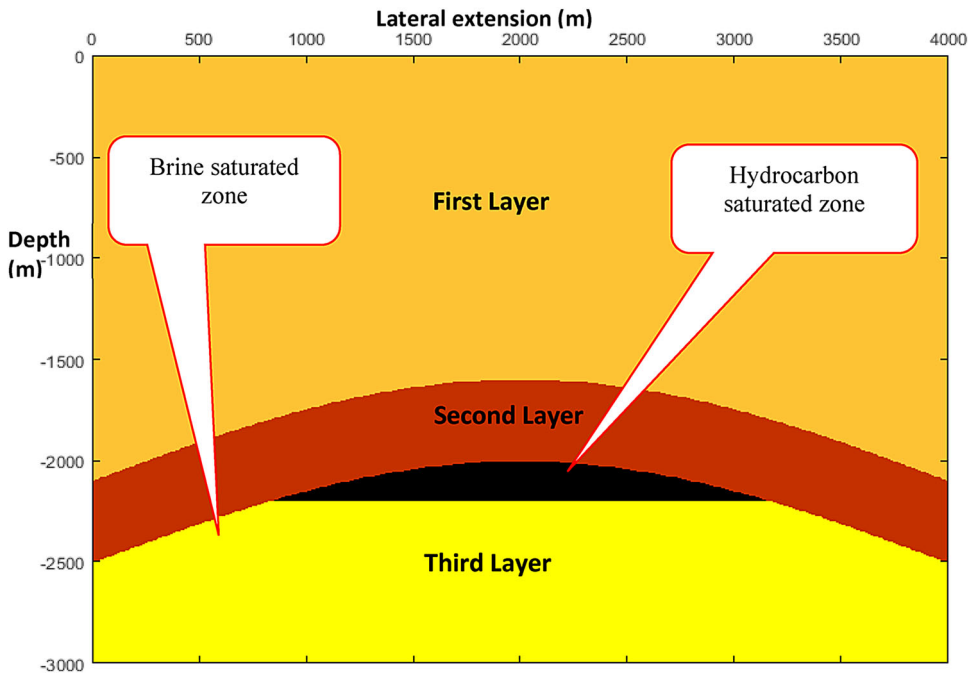

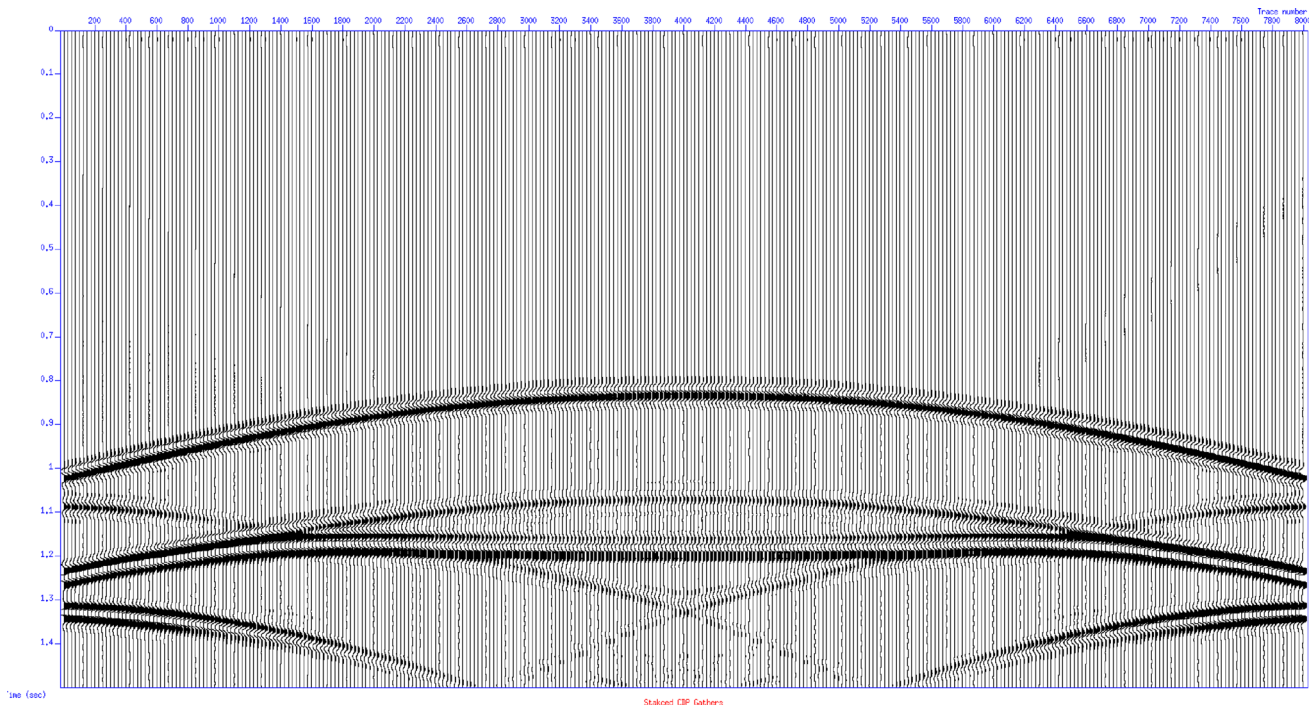

Fig. 3 Synthetic seismic model of three layers geological model

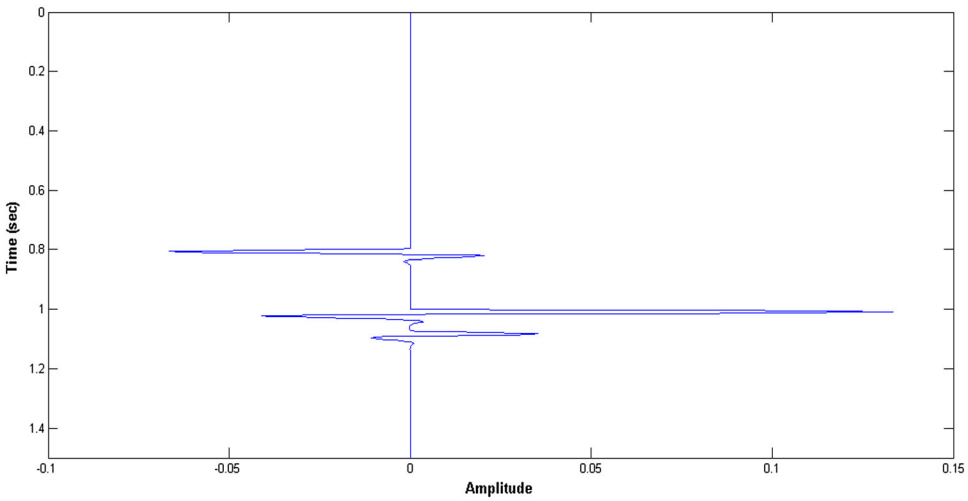

Fig. 4 Seismic trace used in inversion

$$T_r = \frac{T_a}{94.72 + 170.75 \times G} \tag{4}$$

T_a and P are the pressure and temperature at the reservoir level, respectively; and G is the gas/oil ratio, which is in this case 0.56 (methane).

Finally, the density of the gas is computed using following equation (Batzle and Wang 1992):

$$\rho_g = \frac{28.8 \times G \times P}{Z \times R \times T_a} \tag{5}$$

where ρ_g is the density of gas in g/cm^3 and R is the gas constant (which is 8.31441 J/g/mole deg). Z is computed using following equation (Batzle and Wang 1992):

$$Z = aP_r + b + cd \tag{6}$$

where

$$a = 0.03 + 0.00527(3.7 - T_r)^3 \tag{7}$$

$$b = 0.642T_r - 0.007T_r^4 - 0.52 \tag{8}$$

$$c = 0.109(3.85 - T_r)^2 \tag{9}$$

$$d = \mathrm{EXP}\left\{-\left[0.45 + 8 \times \left(0.56 - \frac{1}{T_r}\right)^2\right]\frac{P_r^2}{T_r}\right\} \tag{10}$$

Table 1 Computed properties of gas

S/no.	Property	Value
1.	P (MPa)	21.1600
2.	T_a (K)	423.15
3.	T_r (K)	2.2231
4.	P^r (MPa)	4.5356
5.	Z	0.9858
6.	ρ_g (g/cm^3)	0.0946
7.	m	−0.3996
8.	γ	10.378
9.	f	0.01202
10.	K_g (Pascal)	21960

Table 2 Computed properties of live oil

S/no.	Property	Value
1.	G	0.56
2.	P (GPa)	0.0212
3.	R_g	0.0237
4.	B_o (bbl/STB)	1.1283
5.	ρ' (g/cm^3)	0.7228
6.	ρ_g (g/cm^3)	0.7228
7.	ρ_p (g/cm^3)	0.7229
8.	V_p (m/s)	745.7754
9.	K_o (Pascal)	402040000

Table 3 Computed properties of brine water

S/no.	Property	Value
1.	S (PPM)	84,000
2.	ρ_b (g/cm^3)	1.059628
3.	V_b (m/s)	1499
4.	K_b (Pascal)	2,388,227,392

Table 4 Computed parameters of reservoir fully saturated with gas

Gas		
S/no.	Property	Value
1.	ρ_s (g/cm^3)	2138.93
2.	μ_d (Pascal)	2.25×10^{10}
3.	K_d (Pascal)	1.8×10^{10}
4.	K_s (Pascal)	1.8×10^{10}
5.	V_p (m/s)	4737
6.	K_o (Pascal)	219623.1432

Table 5 Computed parameters of reservoir fully saturated with live oil

Live oil		
S/no.	Property	Value
1.	ρ_s (g/cm^3)	2264
2.	μ_d (Pascal)	2.25×10^{10}
3.	K_d (Pascal)	1.8×10^{10}
4.	K_s (Pascal)	1.849×10^{10}
5.	V_p (m/s)	4627
6.	K_o (Pascal)	402,040,000

Table 6 Computed parameters of reservoir fully saturated with brine water

Brine Water		
S/no.	Property	Value
1.	ρ_s (g/cm^3)	2331
2.	μ_d (Pascal)	2.25×10^{10}
3.	K_d (Pascal)	1.8×10^{10}
4.	K_s (Pascal)	2.07×10^{10}
5.	V_p (m/s)	4663
6.	K_o (Pascal)	2.38×10^9

The bulk modulus of the gas is computed using the following equation (Batzle and Wang 1992):

$$K_g = \frac{P\gamma}{1 - \frac{P_r}{Z} f} \tag{11}$$

where

$$\gamma = 0.85 + \frac{5.6}{P_r + 2} + \frac{27.1}{(P_r + 3.5)^2} - 8.7e^{-0.65(P_r+1)} \tag{12}$$

$$f = cdm + a \tag{13}$$

$$m = 1.2\left\{ -\left[0.45 + 8 \times \left(0.56 - \frac{1}{T_r} \right)^2 \right] \frac{P_r^{0.2}}{T_r} \right\} \tag{14}$$

The results of these equations are given in Table 1.

Live oil properties

The density of the live oil is computed using the following equation (Batzle and Wang 1992):

$$R_g = 0.02123G\left[P\text{EXP}\left(\frac{4.072}{\rho_o} - 0.00377T \right) \right]^{1.205} \tag{15}$$

where R_g is the volume ratio of liberated gas to remaining gas, G is the specific gravity of the gas, it is assumed that methane is dissolved in oil with specific gravity equal to 0.56, T is the temperature, and P is computed for live oil at 2150 m. To get the true density, first a pseudo-density ρ' should be computed using the following equation (Batzle and Wang 1992):

$$\rho' = \frac{\rho_o}{B_o}\left(1 + 0.001R_g\right)^{-1} \tag{16}$$

ρ_o is computed as:

$$\rho_o = \frac{141.5}{\text{API} + 131.5} \tag{17}$$

where API of the live oil is assumed as 42. B_o is the oil formation volume factor that is calculated using the following equation (Batzle and Wang 1992):

$$B_o = 0.972 + 0.00038\left[2.4R_g\left(\frac{G}{\rho_o}\right)^{1/2} + T + 17.8\right]^{1.175} \tag{18}$$

The density of the oil with dissolved gas is given as (Batzle and Wang 1992):

$$\rho_g = \left(\rho_o + 0.0012GR_g\right)/B_o \tag{19}$$

Now this density should be corrected for pressure to find actual density ρ_p as (Batzle and Wang 1992):

$$\rho_p = \rho_g + \left(0.00277P - 1.71 \times 10^{-7}P^3\right)\left(\rho_g - 1.15\right)^2 + 3.49 \times 10^{-4}P \tag{20}$$

The velocity of the live oil is computed using the following equation (Batzle and Wang 1992):

$$V_p = 2096\left(\frac{\rho'}{2.6 - \rho'}\right)^{1/2} - 3.7T + 4.64P + 0.0115\left[4.12\left(1.08\rho'^{-1} - 1\right)^{1/2} - 1\right]TP \tag{21}$$

The bulk modulus of live oil is computed as:

$$K_o = \left(\rho \times V_p\right)10^{-6} \tag{22}$$

The results of these equations are given in Table 2.

Brine water properties

To find the density of brine water, the salinity of water should be known, which is assumed to be 84,000 ppm, and the density of brine of water is computed as (Batzle and Wang 1992):

$$\rho_b = \rho_w + S\{0.668 + 0.44S + 10^{-6}[300P - 2400P \times S + (80 + 3T - 3300S - 13P + 47P \times S)]\} \tag{23}$$

where ρ_b is the density of brine in (g/cm^3), ρ_w is the density of fresh water it is 1 g/cm^3, S is the salinity, T is the temperature, and P is pressure in GPa.

The velocity of brine water is computed as (Batzle and Wang 1992):

$$V_b = V_w + S\left(1170 - 9.6T + 0.055T^2 - 8.5 \times 10^{-5}T^3 + 2.6P - 0.0029TP - 0.0476P^2\right) + S^{1.5}\left(780 - 10P + 0.16P^2\right) - 1820S^2 \tag{24}$$

V_b is the velocity of brine and V_w is the velocity of fresh water which is computed as(Batzle and Wang 1992):

$$V_w = \sum_{i=0}^{4}\sum_{j=0}^{3} w_i T^i P^i \tag{25}$$

where the coefficients w_{ij} are:

$$w_{00} = 1402.85 \quad w_{02} = 3.437 \times 10^{-3}$$
$$w_{10} = 4.871 \quad w_{12} = 1.739 \times 10^{-4}$$
$$w_{20} = -0.04783 \quad w_{22} = -2.135 \times 10^{-6}$$
$$w_{30} = 1.487 \times 10^{-4} \quad w_{32} = -1.455 \times 10^{-8}$$
$$w_{40} = -2.197 \times 10^{-7} \quad w_{42} = 5.230 \times 10^{-11}$$
$$w_{01} = 1.524 \quad w_{03} = -1.197 \times 10^{-5}$$
$$w_{11} = -0.0111 \quad w_{13} = -1628 \times 10^{-6}$$
$$w_{21} = 2.747 \times 10^{-4} \quad w_{23} = 1.237 \times 10^{-8}$$
$$w_{31} = -6.503 \times 10^{-7} \quad w_{33} = 1.327 \times 10^{-10}$$
$$w_{41} = 7.987 \times 10^{-10} \quad w_{43} = -4.614 \times 10^{-13}$$

The bulk moduli of brine water is calculated as

$$K_b = \left(\rho \times V_p\right)10^{-6} \tag{26}$$

The computed properties of brine water are given in Table 3.

The synthetic seismic data are generated using the convolutional model of the seismic trace (Yilmaz 2001). Using following steps, synthetic seismogram for each case was generated. In the first step, AI was computed using the velocity and density of each layer, which was obtained from the density and velocity model (Table 7), and then, it was convolved with zero phase wavelet to generate synthetic seismic trace, AI is computed using the following equation:

$$\text{AI} = V_p \times \rho \tag{27}$$

Table 7 Velocity and density model

S/no.	Property	Value
First layer		
1.	V_p (m/s)	3850
2.	ρ_r (g/cm^3)	2.3
Second layer		
3.	V_p (m/s)	3344
4.	ρ_r (g/cm^3)	2.317
Third layer		
5.	V_p (m/s)	5140
6.	ρ_r (g/cm^3)	2.5

where V_p is the result of seismic data processing.

Gassmann's equation for fluid substitution

Gassmann's equation is well known for fluid substitution to observe the seismic changes. According to this equation, the bulk modulus of a saturated sedimentary rock is given as.

$$K_s = K_d + \frac{\left(1 - K_d/K_m\right)^2}{\frac{\emptyset}{K_f} + \frac{1-\emptyset}{K_m} - \frac{K_d}{K_m^2}} \tag{28}$$

Using published data for matrix bulk modulus (K_m), where K_m is 36.6 GPa (Mavko et al.) for pure sandstone.

K_d and μ_d are computed using Nur et al. (1991, 1995) critical porosity equation as:

$$K_d = K_m\left(1 - \frac{\emptyset}{\emptyset_c}\right) \tag{29}$$

Similarly for μ_d

$$\mu_d = \mu_m\left(1 - \frac{\emptyset}{\emptyset_c}\right) \tag{30}$$

$\emptyset$ and $\emptyset_c$ are porosity and critical porosity, respectively. Every rock type has its own critical porosity, and in this case, for sandstone, it is 0.4, Nur et al. (1991, 1995).

Saturated rock density is calculated using the density-porosity equation, given as follows:

$$\rho_s = (1 - \emptyset)\rho_m + \emptyset\rho_f \tag{31}$$

Gassmann's equation is used for three different fluid substitutions: gas, live oil, and brine water at the reservoir level. Saturated rock modulus, shear modulus, and saturated rock density are used to find the velocity of each fluid as:

$$V_p = \sqrt{\frac{K_s + 4/3\mu_s}{\rho_s}} \tag{32}$$

Tables 4, 5, and 6 list the computed values for all the parameters of gas, live oil, and brine using the above equations, respectively.

Fluid identification

Using the computed velocities and densities of each layer of the model, synthetic seismic data were generated for both cases. From this seismic data, AI and stacking velocity data are calculated. Dix's equation is used to compute the interval velocity.

For AI inversion, the recursive inversion method using the following formula has been used, Becquey et al. 1979:

$$\mathrm{AI}_i = \mathrm{AI}_i\frac{1 + k_i}{1 - k_i} \tag{33}$$

where saturated rock density is computed as:

$$\rho_s = \frac{\mathrm{AI}}{V_p} \tag{34}$$

For the density of the fluid, the density-porosity equation of density log is inverted as:

$$\rho_f = \frac{\rho_s - (1 - \emptyset) \times \rho_m}{\emptyset} \tag{35}$$

here fluid modulus (K_f) is computed by the inverting the Gassmann's equation, as given below:

$$K_f = \frac{\emptyset(K_s - K_d)K_m^2}{[(K_m - K_d)(K_m - K_s) + (K_m \times \emptyset)(K_s - K_d)]} \tag{36}$$

The velocity of the fluid is computed as:

$$V_f = \sqrt{\frac{K_f}{\rho_f}} \tag{37}$$

Results

In this study, three different cases have been investigated, in the first case; the upper portion of the reservoir is fully saturated with gas, which is followed by brine water. In the second case, the uppermost part is saturated with live oil, which is followed by brine water. For the first two cases, porosity is assumed to be 20%. In the third case, this algorithm was applied to Arab-D formation, the main reservoir of Saudi Arabia, with variable porosity, where the uppermost part is saturated with live oil, which is followed by brine water. For the all three cases, AI, fluid density, and fluid velocity inversion have been used to identify the pore fluid in the reservoir.

Cases 1 and 2

AI inversion

Figures 5 and 8 shows the AI plot of the trace, which is exactly in the middle of the model as well as of the reservoir. From 0 to 0.8 s, AI remains the same for the first layer. Then, it starts to decrease from 0.8 to 1 s for the cap rock (shale). As we enter into the reservoir, which is pure sandstone, AI starts to increase from 1 to 1.07 s and the AI reaches up to 1.08749×10^7 kg s/m^2 and $1.0479K10^7$ kg s/m^2, respectively. After 1.07 s, there is a sudden change in AI and it starts to increase again and goes up to 1.08749×10^7 kg s/m^2 (7.3 and 3.8%), respectively, which shows that there are two different pore fluids present in the reservoir (Figs. 6, 7).

Fluid density (ρ_f)

Figures 6 and 9 show the fluid density (ρ_f) plot of the trace, which is exactly in the middle of the model as well as of the reservoir. From 0 to 1 ρ_f has no value because there is no fluid in the upper two layers. As we enter into the reservoir, ρ_f starts to increase from 0 to 95 Kg/m^3 and 0 to 722 Kg/m^3, respectively. Between 1 and 1.07 s, the ρ_f remains the same at 95 kg/m^3 and 722 Kg/m^3, respectively. After 1.07 s, there is a sudden change in ρ_f and it starts to increase again and goes up to 1059 Kg/m^3 (1014.74 and 46.7%), respectively. This shows that we can easily identify pore fluids in the reservoir.

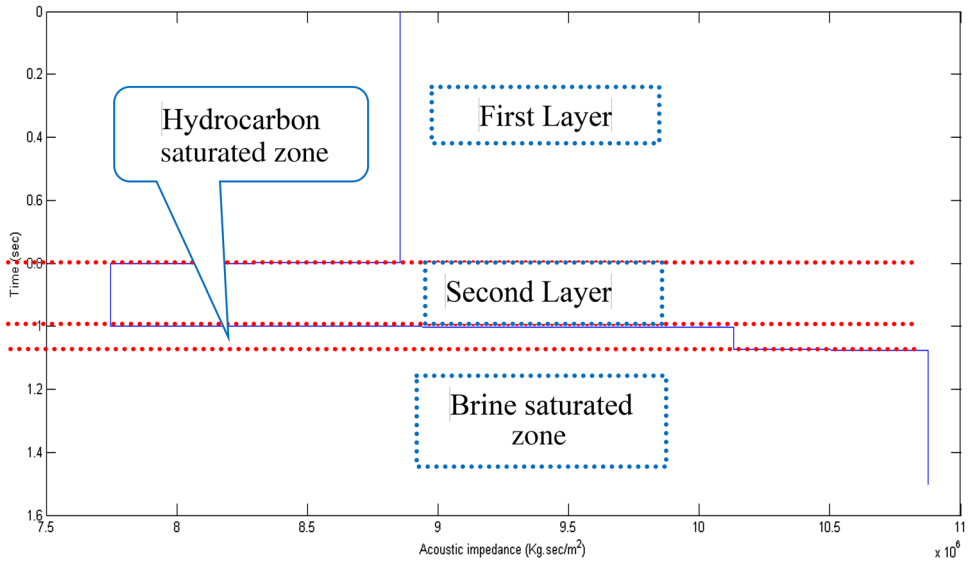

Fig. 5 Acoustic impedance plot of case 1

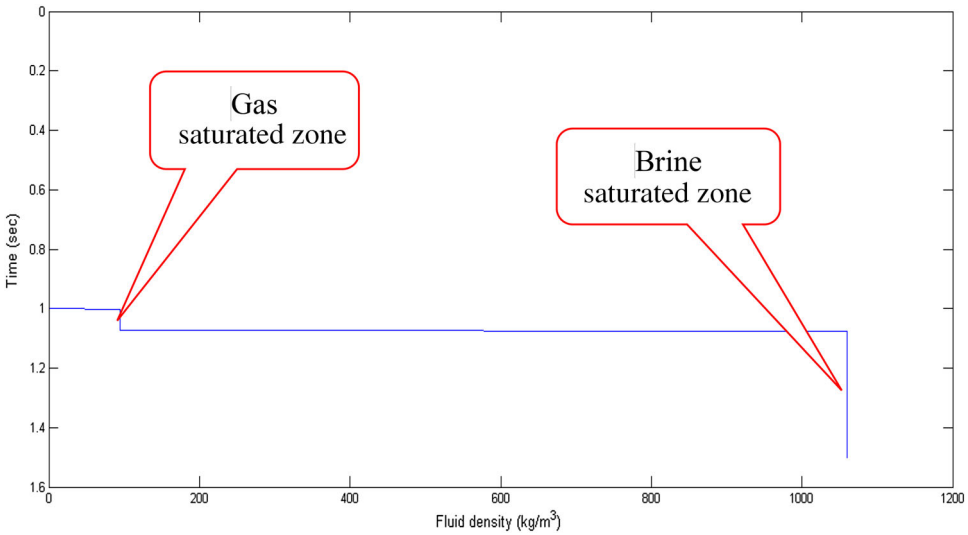

Fig. 6 Fluid density plot of case 1

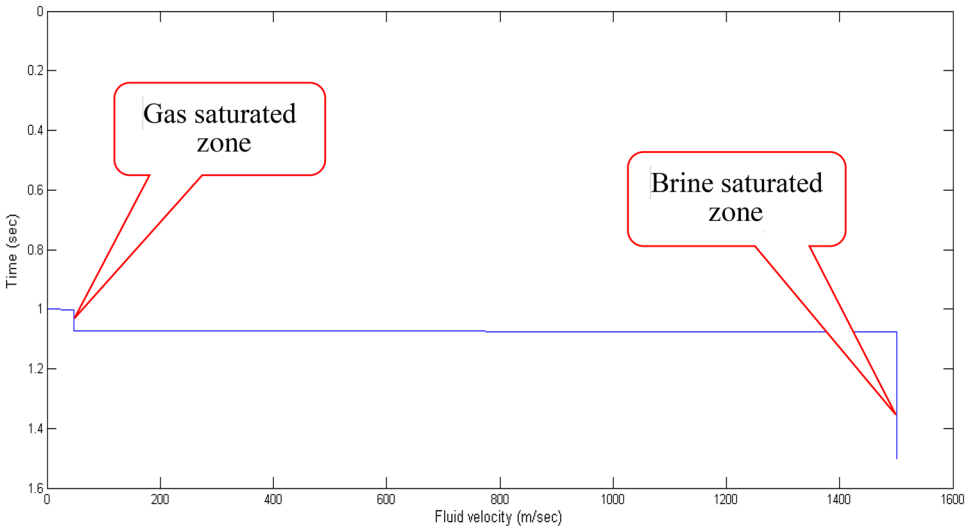

Fig. 7 Fluid velocity plot of case 1

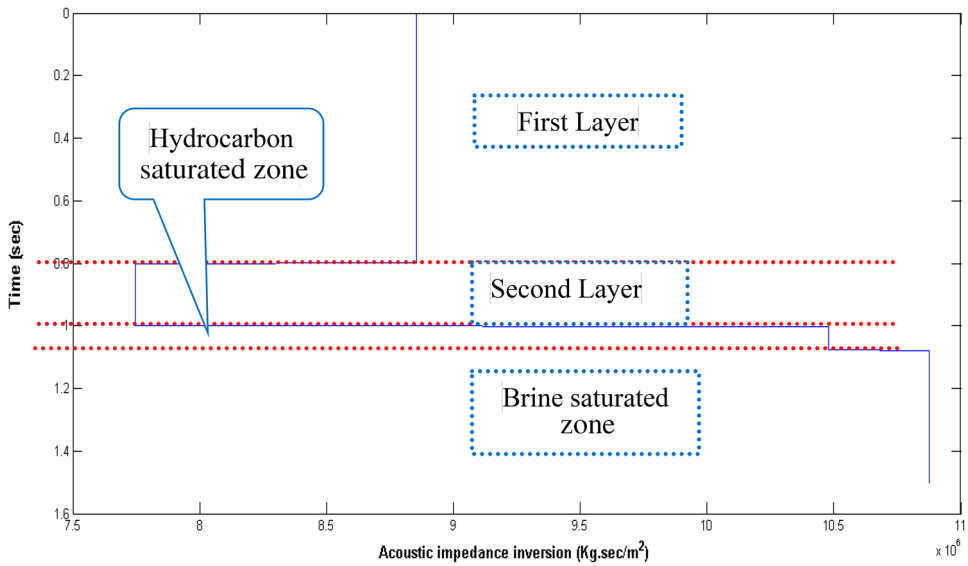

Fig. 8 Acoustic impedance plot of case 2

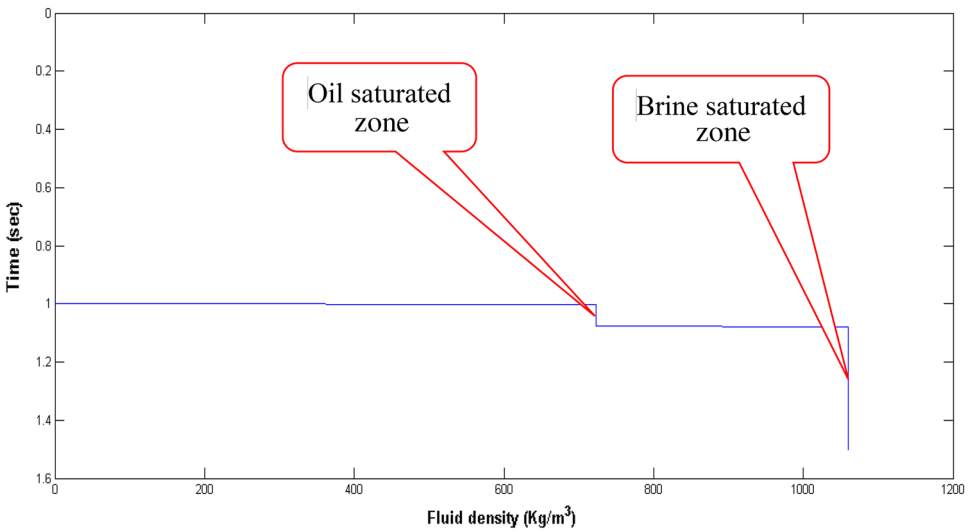

Fig. 9 Fluid density plot of case 2

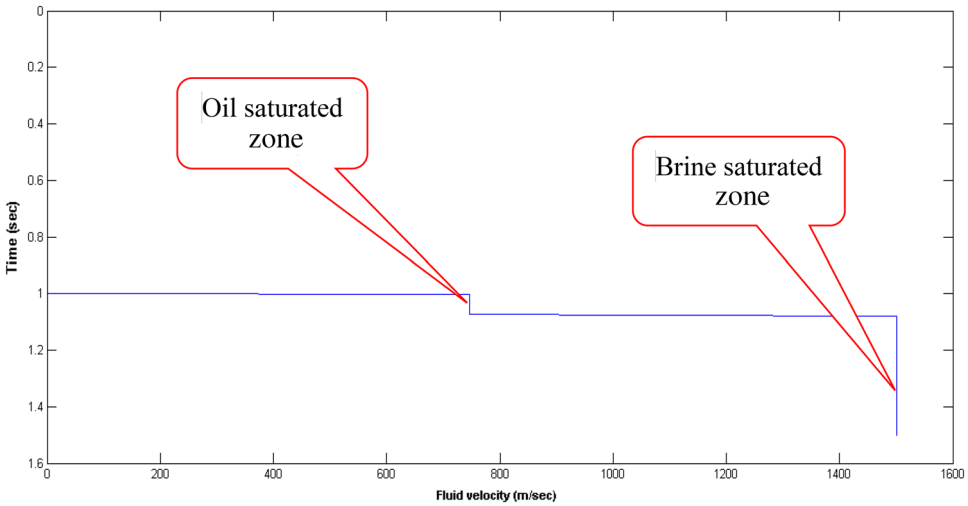

Fig. 10 Fluid velocity plot of case 2

Table 8 Change in percent in AI and ρs

Cases#	Acoustic impedance (%)	Saturated rock density (%)
Case 1	7.30	9.03
Case 2	3.80	3

Table 9 Change in percent in fluid density and fluid velocity

Cases	Fluid density (%)	Fluid velocity (%)
Case 1	1014.74	2900
Case 2	46.70	101.30
Arab formation	46.90	99.00

Fluid velocity (V_f)

Figures 7 and 10 show the fluid velocity (V_f) plot of the trace which is exactly in the middle of the model as well as of the reservoir. V_f has no value because there is no fluid in the upper two layers. As we enter into the reservoir, V_f starts to increase from 0 to 50 and 0 to 745 m/s, respectively, between 1 and 1.07 s and the V_f remains the same at 50 and 745 m/s, respectively. After 1.07 s, then there is a sudden change in V_f and it starts to increase again and goes up to 1500 m/s (2900, 101.3%), respectively. This shows that we can easily identify pore fluids in the reservoir.

Case 3

In the previous two cases, the algorithm worked very well. The only constraint is porosity, which was assumed for the model and was not computed by any means. In case 3, the proposed model will be applied using the published porosity data of the Arab formation.

Steineke et al. (1937) defined the Arab formation as a member of Riyadh formation. Later, Steineke et al. (1958) designated this member as the Arab formation. The type locality of the Arab formation was selected near Riyadh City, but, due to the extensive erosion and weathering, only the subsurface section was assumed the best representation of the Arab formation. The base contact of the Arab formation is with Jubaila limestone, whereas the top contact is with Hith anhydrite. The Arab formation is further divided into four members, which are A, B, C, and D. Although all the members have hydrocarbon potential, Arab D is more prolific. Hith anhydrite provides the seal for the Arab formation. The porosity is different in different members of the Arab formation. Ayres et al. (1982) investigated the porosity in Arab C and Arab D members and found that the porosity ranged from 1 to 30%. In this study, live oil with porosities 10, 20, and 30% has been investigated.

Table 7 is the velocity density model from the eastern part of Saudi Arabia, which is been used to compute the hydrocarbon and brine saturated zones properties (Tables 8, 9).

10% porosity

Fluid density (ρ_f)

Figure 11 shows the fluid density plot of the trace, which is exactly in the middle of the model as well as of the reservoir. To study the effect on fluid density, in this case, the porosity of the Arab formation is assumed to be 10%. From 0 to 1 s, ρ_f has no value because we do not have any fluid in the upper two layers. As we enter into the reservoir, ρ_f starts to increase from 0 to 723 Kg/m^3. Between 1 to 1.07 s, the ρ_f remains at 723 Kg/m^3. After 1.07 s, there is a sudden change in ρ_f and it starts to increase again and goes

up to 1062 Kg/m^3 (46.9%). This shows that we can easily identify pore fluids in the reservoir.

Fluid velocity (V_f)

Figure 12 shows the fluid velocity (V_f) plot of the trace, which is exactly in the middle of the model as well as of the reservoir. In this case, the porosity of the Arab formation is assumed to be 10% to observe the effect on fluid velocity. From 0 to 1 s, V_f has no value because there is no fluid in the upper two layers. As we enter into the reservoir, V_f starts to increase from 0 to 746 m/s, between 1 and 1.07 s the V_f remains at 746 m/s. After 1.07 s, there is a sudden change in V_f and it starts to increase again and goes up to 1481 m/s (98.5%). This shows that we can easily identify pore fluids in the reservoir.

20% porosity

Fluid density (ρ_f)

Figure 13 shows the fluid density (ρ_f) plot of the trace, which is exactly in the middle of the model as well as of the reservoir. In this case, the porosity of the Arab formation is assumed to be 20% to observe the effect on fluid density. From 0 to 1 s, ρ_f has no value because there is no fluid in the upper two layers. As we enter into the reservoir, ρ_f starts to increase from 0 to 723 Kg/m^3. Between 1 to 1.07 s, the ρ_f remains at 723 Kg/m^3. After 1.07 s, there is a sudden change in ρ_f and it starts to increase again and goes up to 1062 Kg/m^3 (46.9%). This shows that we can easily identify pore fluids in the reservoir.

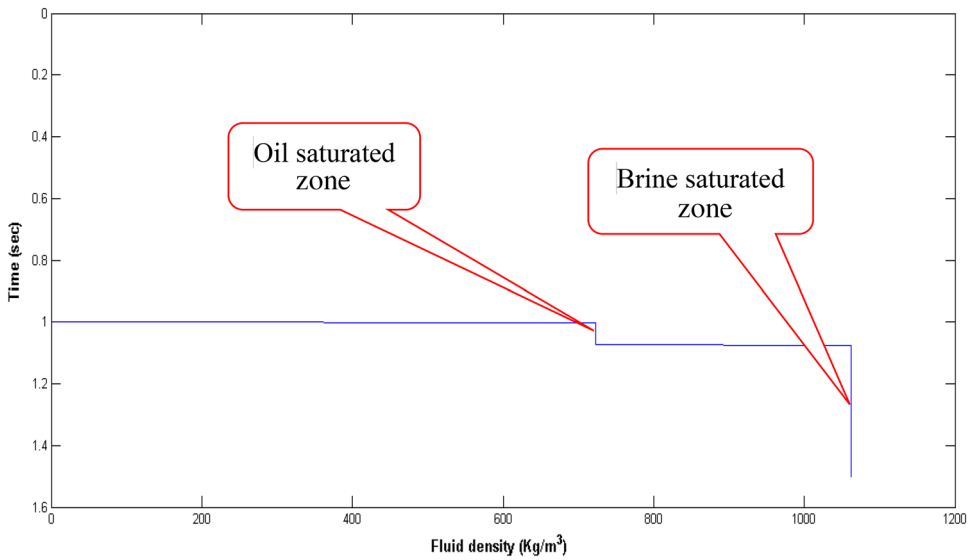

Fig. 11 Fluid density plot with 10% porosity of Arab formation

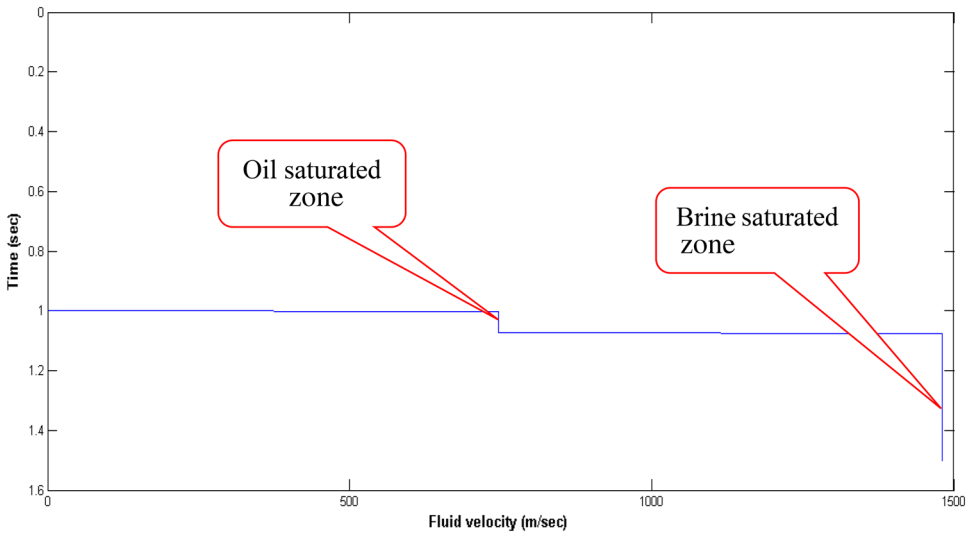

Fig. 12 Fluid velocity plot with 10% porosity of Arab formation

Fluid velocity (V_f)

Figure 14 shows the fluid velocity (V_f) plot of the trace, which is exactly in the middle of the model as well as of the reservoir. In this case, the porosity of the Arab formation is assumed to be 20% to observe the effect on fluid velocity. From 0 to 1 s, V_f has no value because there is no fluid in the upper two layers. As we enter into the reservoir, V_f starts to increase from 0 to 745 m/s, between 1 and 1.07 s the V_f remains at 745 m/s. After 1.07 s, there is a sudden change in V_f and it starts to increase again and goes up to 1492 m/s (100.3%). This shows that we can easily identify pore fluids in the reservoir.

30% porosity

Fluid density (ρ_f)

Figure 15 shows the fluid density (ρ_f) plot of the trace, which is exactly in the middle of the model as well as of the reservoir. In this case, the porosity of the Arab formation is assumed to be 30% to observe the effect on fluid density. From 0 to 1 s, ρ_f has no value because we do not have any fluid in the upper two layers. As we enter into the reservoir, ρ_f starts to increase from 0 to 723 Kg/m^3. Between 1 to 1.07 s, the ρ_f remains at 723 Kg/m^3. After 1.07 s, there is a sudden change in ρ_f and it starts to increase again and goes up to 1062 Kg/m^3 (46.9%). This shows that we can easily identify pore fluids in the reservoir.

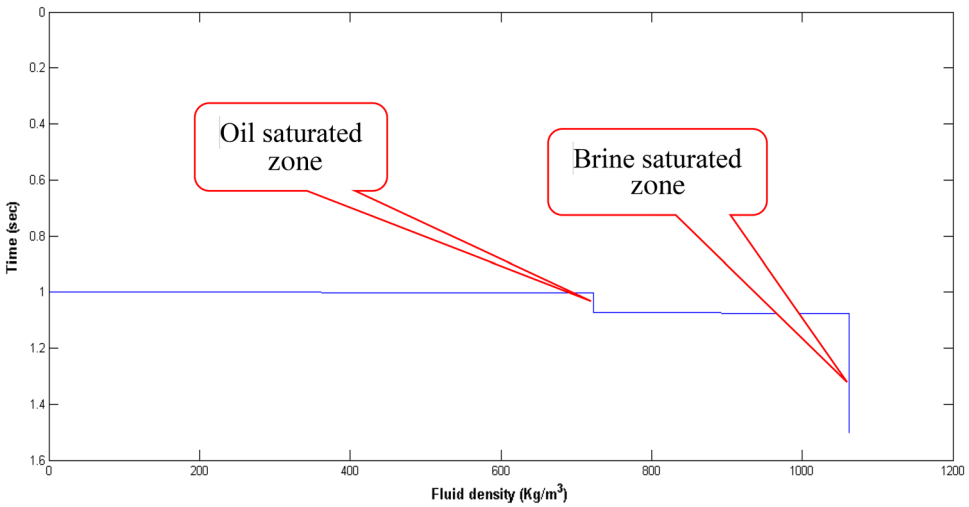

Fig. 13 Fluid density plot with 20% porosity of Arab formation

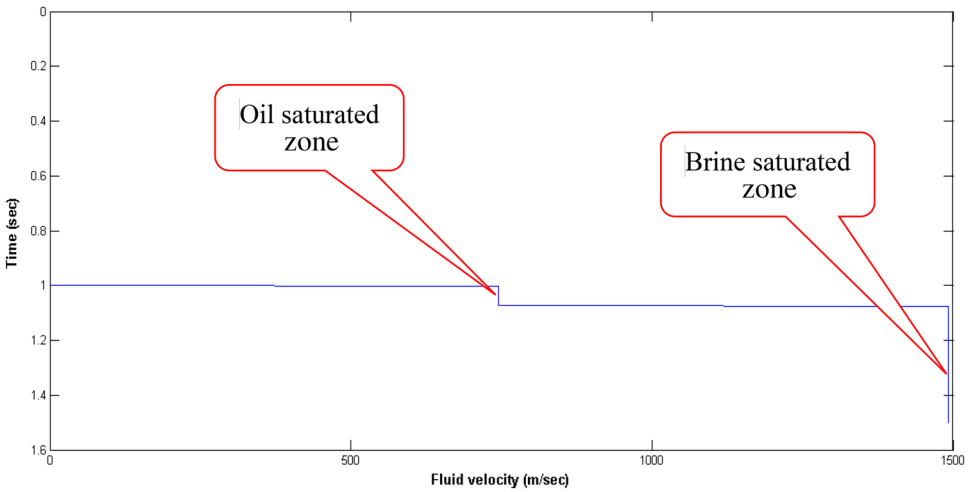

Fig. 14 Fluid velocity plot with 20% porosity of Arab formation

Fluid velocity (V_f)

Figure 16 shows the fluid velocity (V_f) plot of the trace, which is exactly in the middle of the model as well as of the reservoir. In this case, the porosity of the Arab formation is assumed to be 30% to observe the effect on fluid velocity. From 0 1 s V_f has no value because we do not have any fluid in upper two layers. As we enter into the reservoir, V_f starts to increase from 0 to 748 m/s, between 1 and 1.07 s the V_f remains at 748 m/s. After 1.07 s, there is a sudden change in V_f and it starts to increase again and goes up to 1490 m/s (99.2%). This shows that we can easily identify pore fluids in the reservoir.

In the case of the Arab formation, where we have different porosities, the percent error in fluid density is given in Table 2.

Conclusions

This study has investigated the effects of pore fluids on seismic data in order to characterize the pore fluid. Characterization of fluids at reservoir level by using seismic data in the absence of well logs data is a very helpful tool for reserves estimation before drilling new wells and will increase chances of success.

Three different scenarios have been studied to identify the pore fluid in the target reservoir with few assumptions on synthetic seismic data. In first two cases, AI inversion gave good evidence of the presence of two different pore fluids in the reservoir. Results of fluid density and fluid velocity gave good evidence and information about the pore fluids and are a helpful tool in identifying the pore fluids in the reservoir. The percent error between the inverted fluid density/velocity and the computed fluid density/velocity for gas, live oil, and brine is almost 0% for cases 1 and 2. The same approach was also applied to synthetic seismic traces representing the Arab formation of

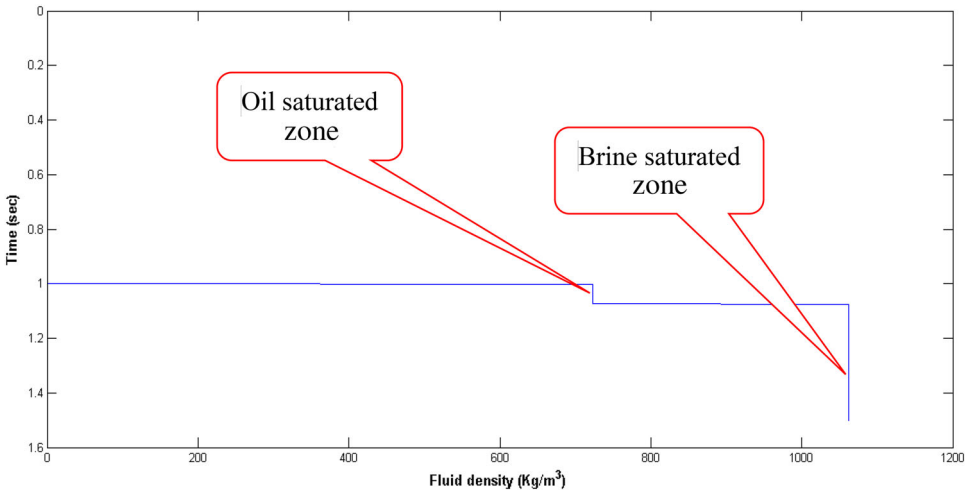

Fig. 15 Fluid density plot with 30% porosity of Arab formation

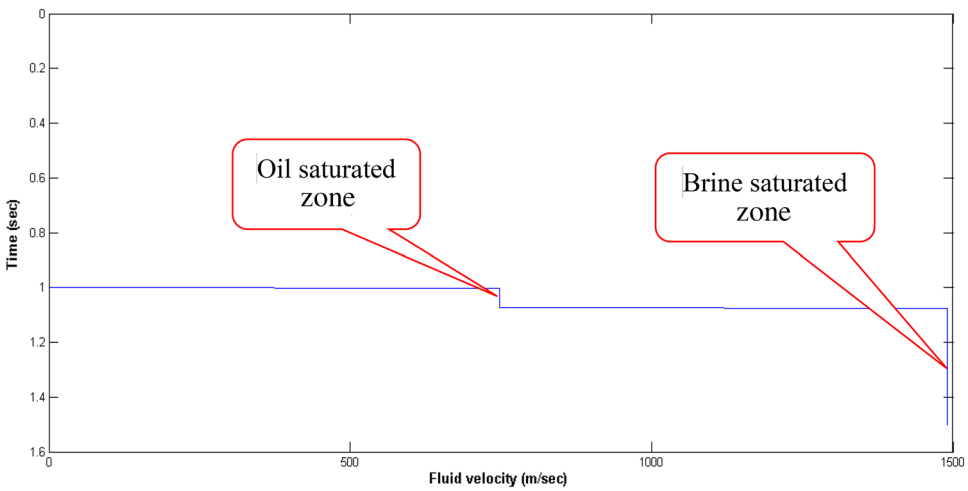

Fig. 16 Fluid velocity plot with 30% porosity of Arab formation

Table 10 Percent error analysis in the Arab formation

Fluid type	Porosity (%)	Computed fluid density (Kg/m^3)	Inverted fluid density (Kg/m^3)	Percent error	Computed fluid velocity (m/s)	Inverted fluid velocity (m/s)	Percent error (%)
Live oil	10	722.9	723	0.0138	745.7754	746.7897	0.136
	20		723	0.0138		745.7225	0.096
	30		723	0.0138		748.1047	0.3123
Brine	10	1059.624	1062	0.2238	1499	1481.383	1.175
	20		1062.5	0.2714		1492.46	0.436
	30		1062.333	0.2556		1490.372	0.5755

Saudi Arabia within a range of porosities. The inversion of these cases also results in a similarly small error between the inverted and true fluid properties.

The results of this study revealed that:

- AI, fluid density, and fluid velocity inversion gave good evidence of the presence of two different pore fluids in the reservoir due to sudden change as we moved from the upper zone to the lower zone within the reservoir.
- The results of fluid density and fluid velocity give better evidence and information about the pore fluids and are a helpful tool in identifying the pore fluids in the reservoir.
- The percent error between the inverted fluid density and velocity and the computed fluid density and velocity for gas, live oil, and brine is almost 0% for cases 1 and 2.
- The percent error for Arab formation for different porosity is given in Table 10, where the maximum percent error we have is 1%.

References

Archie GE (1942) The electrical resistivity log as an aid in determining some reservoir characteristics. SPE 146:54–62

Ayres MG et al (1982) Hydrocarbon Habitat in Main Producing Areas, Saudi Arabia. AAPG Bull 66(1):1–9

Batzle M, Wang Z (1992) Seismic properties of pore fluids. Geophysics 57(11):1396–1408

Becquey M, Lavergne M, Willm C (1979) Acoustic impedance logs computed from seismic traces. Geophysics 44(9):1485–1501

Chi XG, Han DH (2007) Reservoir properties inversion from AVO attributes. In: SEG technical program expanded abstracts 2007, p 1868–1872

Chiburis E (1987) Studies of amplitude versus offset in Saudi Arabia, In: SEG technical program expanded abstracts 1987, Society of Exploration Geophysicists. p 614–616

Chombart L (1960) Well logs in carbonate reservoirs. Geophysics 25(4):779–853

Gevers ECA, Watson SW (1978) Quantative interpretation of seismic data using well logs. Society of Petroleum Engineers, SPE, Houston

Kato A, Stewart R (2012) Joint AVO inversion for time-lapse elastic reservoir properties. Society of Petroleum Engineers, SPE, Houston

Klimentos T (1995) Attenuation of P- and S-waves as a method of distinguishing gas and condensate from oil and water. Geophysics 60(2):447–458

Li D, Zhang F (2015) Direct estimation of petrophysical properties based on AVO inversion. In: SEG technical program expanded abstracts 2015. p 2886–2890

Nur AM et al. (1995) Critical porosity: the key to relating physical properties to porosity in rocks. In SEG technical program expanded abstracts 1995, p 878–881

Rosa ALR, Arso LR, Jaegher R (1985) Mapping oil–water contact with seismic data in Campos Basin, Offshore Brazil. In: SEG technical program expanded abstracts 1985, p 441–442

Snyder D, Fleming D (1985) Well logging—a 25-year perspective. Geophysics 50(12):2504–2529

Steineke M, Bramkamp RA, Sander NJ (1958) Stratigraphic relations of Arabian Jurassic oil in Habitat of oil. In: American association petroleum geologists symposium, p 1294–1329

Williams DM (1990) Mobil Research and Development Corporation 1990-W SPWLA Conference Paper. Society of Petrophysicists and Well-Log Analysts, Louisiana

Yilmaz O (2001) 1. Fundamentals of signal processing, in seismic data analysis. 2001, Society of exploration geophysicists. p 25–158

Publisher's Note